2014 IEEE International Conference on Robotics & Automation (ICRA)
Hong Kong Convention and Exhibition Center
May 31 - June 7, 2014. Hong Kong, China

A Novel 4-DOFs Origami Enabled, SMA Actuated, Robotic End-effector for Minimally Invasive Surgery

M. Salerno, *Student Member, IEEE*, K. Zhang, *Member, IEEE*, A. Menciassi, *Member, IEEE* and J. S. Dai, *Member, IEEE*

***Abstract*— Minimally invasive Surgery (MIS) is one of the most challenging fields for robot designers due to the limited size of the access points, to the high miniaturization level and to the dexterity needed for performing surgical tasks. For this reason, the integration of actuators should proceed in parallel with the identification of the most effective transmission mechanisms and kinematics. Conversely, only a few microfabrication technologies are adequate for developing small size mechanisms with safe operation in the human body. In this paper a SMA actuated, miniaturized, origami-enabled, parallel structure is presented as a versatile module for novel robotic tool in MIS, the parallel structure has been combined with a twisting module and a gripper obtaining a 4-DOFs on board actuated end-effector.**

I. Introduction

Minimally invasive surgery (MIS) is considered nowadays one of the most promising trends for surgical procedures, MIS aims to minimize the access and the mechanical interactions with the body and to focus on the interventional area by deploying surgical instruments through harmless paths.

By following these guidelines, minimally invasive techniques relieve post-operative pain, shorten hospital stays, improve cosmetics and decrease morbidity [1].

However, the execution of procedures with the MIS approach is very challenging due to the high dexterity needed to perform surgical tasks and being limited the mobility and stability of current surgical tools passing through small size access points [2].

For these reasons, in order to satisfy MIS constraints, novel surgical instruments, tools and robotic platforms are under continuous development and receive much attention. In particular, surgical robots are evolving in order to be efficiently delivered in the interventional area thus providing the high dexterity, [3], [4].

* Research supported by the by the STIFF-FLOP project grant from the European Communities Seventh Framework Programme under grant agreement 287728 and by TOMSY project grant from the European Communities Seventh Framework Programme under grant agreement 270436.

M. Salerno is with The BioRobotics Institute of Scuola Superiore Sant'Anna, Pisa 56127 ITALY (phone: 0039-050883017; fax: 0039-050883 402; e-mail: m.salerno@sssup.it).

K. Zhang is with the CORE, King's College London, Strand, London, WC2R 2LS United Kingdom (phone: 0044-2078482428; e-mail: ketao.zhang@kcl.ac.uk).

A. Menciassi is with The BioRobotics Institute of Scuola Superiore Sant'Anna, Pisa 56127 ITALY (e-mail: a.menciassi@sssup.it).

J. S. Dai. is with the CORE, King's College London, Strand, London, WC2R 2LS United Kingdom (e-mail: jian.dai@kcl.ac.uk).

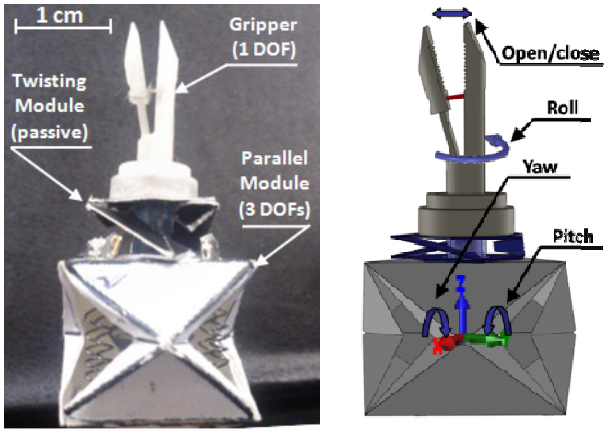

Figure 1. 4 DOFs origami enabled SMA actuated miniaturized end-effector. Real prototype and system components (left), 3D design and system DOFs (rigth).

Recent achievements are represented by steerable concentric robots [5] and by modular/snake-like robots that can provide very high dexterity due to their high number of degrees of freedom (DoFs).

In these systems, modularity combined with cable or rod actuation allows a good miniaturization level, [6]; furthermore these platforms are quite flexible and can be employed in different anatomical districts for a variety of pathologies requiring different access points [7], [8].

Following the indications provided by leading users (i.e. medical doctors and surgeons) about design and introduction of robots in the operative room, miniaturization, low weight and small footprint should be the main features of new generations of surgical robots [9].

Unfortunately, miniaturization and lack of adequate actuation and transmission mechanisms usually lead to simplification of the system thus reducing its dexterity, especially at the end-effector (the most distal component of the robot [9]). Defining a tradeoff between mechanism complexity and platform miniaturization is quite challenging; for this reason snake-like modular robots represent an attractive solution [10] since they compensate limited complexity of a simple module with redundancy of many modules.

Alternative actuation strategies, respect to externally actuated cables and NiTi backbones, have some advantages; for example embedding the actuators inside the robot body (on-board), the platform footprint is reduced and the need of transmission elements running in the whole robot structure is minimized [4], [9]. In addition to miniaturization and distal actuation, the trend to minimize patient trauma led some research groups in designing minimal access robots that are intrinsically safe. These robots, composed by soft structures

embedding compliant actuators, would adapt their shape to the environment in order to safely interact with human anatomy during both deployment and operation tasks [11]; the employment of muscle-like actuators such as shape memory alloys (SMA) or flexible fluidic actuation can preserve platform inherent compliance as demonstrated in the design of robots mimicking biological soft structures [12].

In recent years, emerging fabrication techniques have demonstrated their efficiency in the development of miniaturized soft robotic systems preserving flexibility when integrated in more complex system. These techniques carry many advantages in terms of reduced wirings (i.e. electrical connections, sensors and actuators can be embedded in the structure as part of the fabrication process), fabrication accuracy and small scale efficiency [13]. In particular, Smart Composite Microstructure (SCM) fabrication method takes advantage of the high accuracy obtainable by 2D laser cut to define planar structure that can be folded for generating 3D complex structures [14]. Based on this consideration, origami represents a source of inspiration in miniaturized system design due to their capability to replicate complex joints behavior [15]. Origami structures are quite cost effective when fabricated with SCM technique and they are ideal for small scale (<cm) applications where surface effects dominate: multi components joints are inefficient and too complex to realize, while 3D arrangements of rigid planes and flexible hinges can provide equivalent constraints [14], [15].

From the actuation point of view, SMA represents one of the most widely employed technologies in medical instruments [16] due to their unique pseudoelastic features and shape recovery capabilities. Further, in addition to piezomotors and pneumatic or hydraulic actuation systems that are more common due to their high speed and frequency actuation capabilities, SMA actuators are one of the preferred technologies in magnetic resonance imaging (MRI) compatible instruments and robots [17].

SMAs allow the design of very compact and compliant actuators with a very high power-to-weight ratio; actuators performances can be tuned by annealing the alloy in different shapes while transition temperature depends on alloy composition. SMAs could be an ideal solution for origami actuation, since they can be easily embedded in a complex structure providing high forces and wide deformations ranges in a very small volume.

The effective combination of tool dexterity, adequate workspace, distal actuation, safe operation and miniaturization is the main challenge in designing robots for MIS. For this reason, the integration of actuators should proceed in parallel with the identification of the most effective transmission mechanisms and kinematics. Conversely, only a few microfabrication technologies are adequate for developing small size mechanisms with safe operation in the human body.

In this paper, the proof of concept of a SMA actuated, miniaturized, origami-enabled, parallel structure is presented. The proposed structure presented as a versatile module for novel robotic tool in MIS, has been integrated with a twisting module and a gripper obtaining a 4 DOFs miniaturized end-effector with on board actuators as illustrated in Fig. 1.

The features of the parallel structure, and the actuation system design have been reported in section II, while testing and performance evaluation are addressed in section III. Finally, conclusions and future work are reported in section IV.

II. Materials and Methods

A. Parallel foldable structure

One of the most attractive features of origami structure is the possibility to design the kinematics and stiffness of the mechanism to maintain specific directions in which the whole structure can be completely folded, thus providing inherent compliance to the system.

Origami qualities match very well with surgical robotics requirements, but one of the most important advantages is the possibility to shrink the structure to very small size complex designs limiting the need of a tradeoff between mechanism complexity and platform miniaturization and leaving freedom in systems design with much less limitations for robots dexterity.

The employed foldable parallel structure, presented by Zhang in [18], is composed of three spherical six-bar kinematic chains by connecting a triangular shaped base and a platform as shown in Fig. 2a.

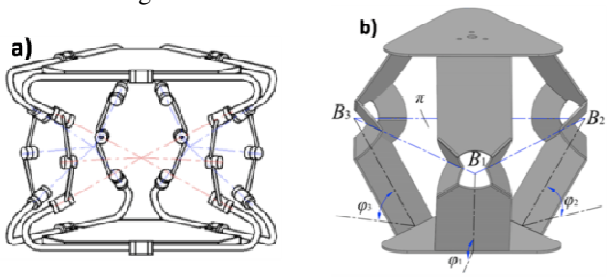

Figure 2. 3 DOFs origami enabled parallel platfrom. Linkage and 1 DOF rotational hinges platform assembly (left). Equivalent platform obtained folding a 2D rigid planes and flexible hinges (rigth).

The described arrangement of 1 DOF rotational joints and system symmetry, generate a 3 DOFs parallel platform whose kinematics is based on the virtual symmetric plane (π) defined by the centers of the three spherical chains.

By actuating the angles φ_1, φ_2 and φ_3 between the base plane and the links of the kinematic chain connected to the base, as described in Fig. 2b, rotations and translations can be applied to the platform; available DOFs and the workspace (relative to a platform composed by a 20 mm side triangular base) are reported in Fig. 3.

Origami technique makes it possible to obtain the described three-dimensional structure by erecting and folding a 2D arrangement of rotational joints (origami creases) and planar links. The compact design of the platform allows very small size changes during motion due to the hollow internal volume that accommodates the different configurations of the links. Further, the hollow space can be exploited to embed a channel for an interchangeable endoscopic tool. Respect to other literature solutions, the proposed module has the advantage of providing rotations up to 45 degrees, wider than 10 degrees of the module reported in [4] or 90 degrees of the whole continuum robot reported by [19] and provides a squeezing degree of freedom that can be exploited as

translational DOF or converted to a rotational DOF of a gripper by integrating a passive twisting module proposed in this paper.

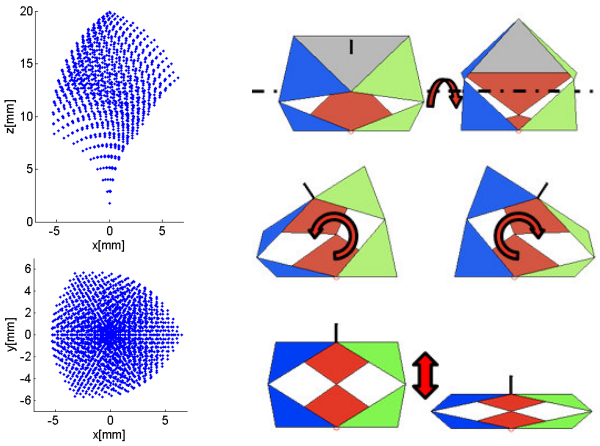

Figure 3. Parallel foldable structure workspace (left) and degrees of freedom (rigth): two rotational (top and central) and one translational (bottom).

B. Gripper design

The gripper has been placed in the top of the system as illustrated in Fig. 1. Its design consists of a simple compliant structure to be coupled to a linear actuator. The compliant gripper is connected to a SMA actuator with a cable designed to exert a normal force to the flexible beam. Finite elements analyses and experimental tests have been conducted in order to define and verify its range of motion and the force required for its actuation. Gripper design and it force/deflection curve are reported in Fig. 4.

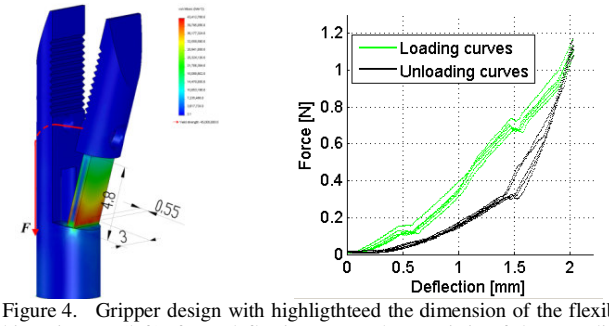

Figure 4. Gripper design with highligthteed the dimension of the flexible hinge in mm (left), force deflection curve characteristic of the compliant gripper.

In order to provide a rotational DOF to the gripper, the translational motion of the parallel structure in Fig. 3 has been converted by exploiting the novel 1 DOF three-legged parallel mechanism (twisting module) with a virtual central shaft illustrated in Fig. 5.

The proposed twisting module employs only rotational joints and the three legs are symmetrically distributed.

According to the geometry of the joints axes in the chain legs, the platform of the parallel mechanism is constrained by three constraint forces exerted by the three legs; the three constraint forces are lying on a hyperboloids of revolution about the axis *OO'* joining the base and platform centers.

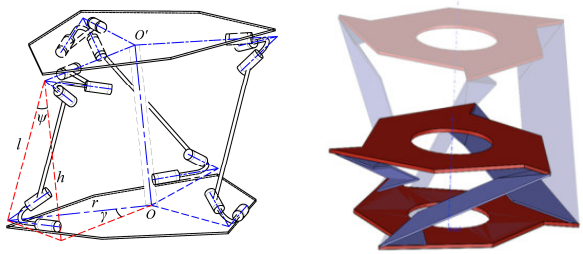

Figure 5. 1 DOFs origami enabled twisting module. Linkage and 1DOF rotational hinges platform assembly (left). Equivalent platform obtained folding a 2D rigid planes and flexible hinges (rigth).

Due to the additional constraint provided by the hollow shaft passing through *O* and *O'* and connecting the gripper to the parallel module, the motion of the proposed twisting module is restricted to 1 DOF screw motion with axis *OO'*.

Hence, the twisting module acts as a passive structure converting the translational squeezing motion of the parallel structure into a rotational motion of the gripper.

According to the structure of the passive twisting module and the screw motion, the twisting angle of the platform with respect to the base of the mechanism can be derived as

$$\gamma = 2\arcsin\left(\frac{\sqrt{l^2 - h^2}}{2r}\right) \quad (1)$$

where γ is the twisting angle of the platform, l is the length of the chain leg and h is the vertical distance between the platform and the base.

Since the gripper rotation angle is dependent on the parallel module squeezing translational movement d, (as described in Fig. 5 and 6), Eq. (1) becomes:

$$\gamma = 2\arcsin\left(\frac{\sqrt{l^2 - (l-d)^2}}{2r}\right) \quad (2)$$

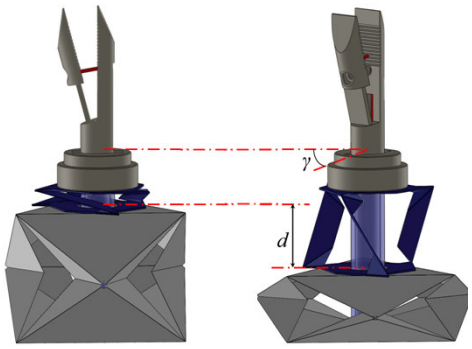

Figure 6. The proposed twisting module, enables the conversion of parallel module translational degree of freedom into a rotational DOF of the gripper, the width of the rotation γ is dependent by the sqeezing range d.

C. Actuation system design

For their unique features SMAs are very good candidate for miniaturized compliant robotic systems, but unfortunately they have many drawbacks: since their activation is initiated by a temperature transition (usually obtained by joule effect) and since it highly depends by the thermal exchanges with the environment, their control is challenging and their actuation speed and frequency is quite limited. The alloy presents hysteresis during activation/deactivation phases and overheating compromises actuators functionalities.

However, recent works incremented the knowledge and usability of these actuators, defining more efficient and accurate models [20] and design methods. Literature works

investigated the possibilities to obtain sensorless feedback for SMA linear actuators in helical spring shape exploiting the measurements of the inductance relative to actuators geometry [21], thus minimizing the components to integrate in the robot. Small scale robots (< cm) are ideal for SMA applicability since surface phenomena become predominant respect to volume ones improving thermal exchanges therefore incrementing actuators performance. Moreover, specific mechanisms can be designed in order to overcome some drawbacks typical of SMA actuator systems i.e. the biologically inspired mechanism embedded in the jumping robot proposed by Kim et al [22] provides high speed actuation exploiting SMA actuators used to release suddenly an elastic element.

In this work, SMA actuators have been embedded in the previously described parallel structure in order to demonstrate the feasibility of a 4 DOFs origami enabled end-effector.

In order to simplify the system design, the actuators able to maximize the squeezing DOF with a synchronous actuation have been identified, while the maximum obtainable angular motion has been verified experimentally (see Section III).

Since the parallel module has been obtained by folding a 0.3 mm thick paper sheet, a steel helical compression spring (wire diameter 0.58 mm, external diameter 9.2 mm, spring height 15 mm and 3 active coils for a resulting spring constant of 0.59 N/mm) connecting the base and the platform has been employed to provide elasticity to the structure.

The elasticity of the system during axial compression motion has been then characterized by experimental tests in order to evaluate the influence of the parallel structure on the steel spring behavior (Fig. 7).

For both structure elasticity and SMA actuators characterization, a strain stress setup composed by a linear stage interfaced to a brushless motor and a ATI nano17 force torque sensor has been exploited.

The strain stress curve resulting by 10 cyclic solicitations of 2 different prototypes has been reported in Fig. 7 (right). The static two-state model, proposed by An et al [20] able to describe nonlinearities induced by martensite detwinning phase and the by helical spring large deformations, has been implemented and experimental tests on SMA helical springs have been conducted in order to retrieve the characteristics parameters.

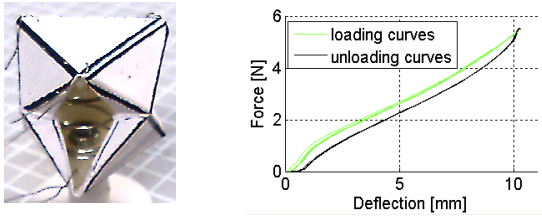

Figure 7. Steel helical compression spring connecting the top and the base of the parallel module (left). Force deflection curves of the parallel module during compression tests (rigth).

The SMA actuators have been manufactured constraining SMA wires (Flexinol by Dynalloy, CA, USA) around a steel rod and annealing the alloy at a temperature of 500 °C for 15 minutes; the geometric parameters of the tested SMA helical spring, are reported in Table I.

The SMA strain stress curves in austenite and martensite phases superimposed with model results are reported in Fig. 8 while in Table II have been summarized the SMA retrieved parameters:

- G_A and G_M, the shear modulus in austenite and martensite conditions
- τ_A^{Cr} the maximum shear stress in austenite phase
- τ_s^{Cr} the shear stress corresponding to the beginning of stress induced detwinning process
- τ_f^{Cr} the shear stress corresponding to the end of stress induced detwinning process
- γ_L the maximum residual strain γ

TABLE I. PARAMETERS OF SMA HELICAL SPRING SPECIMEN FOR OBTAINING ACTUATOR PROPERTIES

Spring index[a]	*Wire diameter [μm]*	*Spring diameter[mm]*	*N° of turns*
7	200	1.4	17

a. The spring index is defined as the spring diameter-to-wire diameter ratio

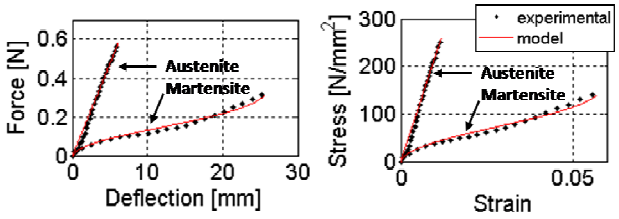

Figure 8. Force/deflection and stress strain curves of the SMA tested coil experimental and model comparison.

TABLE II. PROPERTIES OF THE SMA COIL SPRING ACTUATOR

In $A_{100\%}$ state	G_A *[GPa]*	τ_A^{Cr} *[MPa]*		
	22	260		
In $M_{100\%}$ state	G_M *[GPa]*	τ_s^{Cr} *[MPa]*	τ_f^{Cr} *[MPa]*	γ_L
	8.15	10	140	0.04

Once obtained the model parameters, the dimensional constraints for the actuators, (maximum external diameter and maximum length of the spring) have been identified.

The possibility of placing a single actuator (SA) or two actuators in parallel configuration (PA) in each corner of the platform, as shown in Fig. 9, has been considered.

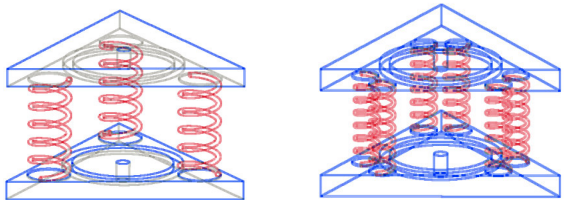

Figure 9. Possible SMA helical spring arrangement in the parallel module. Single actuator solution consisting in three actuators (left). Parallel actuator solution consisting in six actuators (rigth).

In order to identify the most appropriate design parameters, the platform elastic characteristic has been compared with an analytical model of the SMA actuator [20] varying its design parameters (i.e. wire diameter, spring diameter, number of active coils).

The most performing solution for single actuator and for the actuators in parallel configuration have been identified, the graph describing the coupling of the actuators with the bias element is reported in Fig. 10 while the actuators features are and reported in Table III.

In order to simplify the system design, the hysteresis induced by the structure material has not been considered employing a mean curve in between loading and unloading. The simulations were implemented exploiting a MATLAB (MathWorks, USA) routine and the resulting design possibilities have been sorted in order to maximize actuation range.

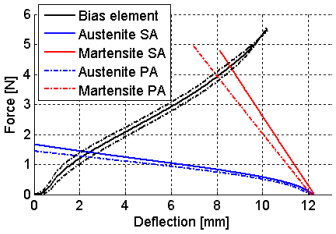

Figure 10. SMA actuators /bias element coupling referred to the steel spring reference system.SA configuration shows lower actuation range respect to PA configuration.

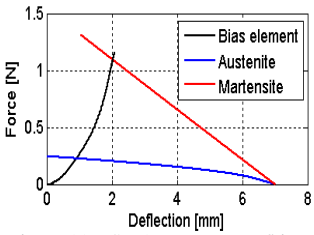

Figure 11. SMA actuators /bias element coupling referred to the steel spring reference system.SA configuration shows lower actuation range respect to PA configuration.

The method described for the parallel module actuation design, has been employed for the gripper actuators design.

The SMA spring, used to actuate the gripper, has been placed inside a flexible PTFE tube (inner diameter of 2.5 mm, external diameter of 4 mm and length of 22 mm) playing the role of shaft connecting the gripper to the base of the parallel module and passing through the twisting module. In order to obtain 15deg of gripper open/close range, the compliant system has to be actuated according to the average of the curves reported in Fig. 4. However, the employed material viscoelasticity produced an important hysteresis; the use of a metal material for the gripper, such as titanium or beryllium-copper (MR compatibles) should drastically improve the gripper behavior thanks to more predictable properties of the material.

The parameters of the actuator satisfying the design constraints and providing the wider actuation range for the gripper actuation (GA), are reported in Table III.

TABLE III. SMA HELICAL SPRING ACTUATION FEATURES

	Spring index[a]	*Wire diameter [µm]*	*Spring diameter[mm]*	*N° of turns*	*Actuation range [mm]*
PA	8	250	2	7	6.2
SA	8.7	375	3.25	5	5.9
GA	5	300	2.1	11	1.1

a. The spring index is defined as the spring diameter-to-wire diameter ratio

D. System integration and performance evaluation

The various components composing the 4-DOFs end-effector, have been initially tested separately in order to distinguish the performance of each component. Successively, the proposed device has been assembled and the components jointed performances have been obtained.

The parallel structure has been assembled (see the companion video for details) embedding the actuators (Fig. 12 left) and it has been connected to three independent PWM driven current generator circuits. The PWM signal has been generated by an ARDUINO UNO board (Arduino, Italy) the actuation command has been acquired by a joystick, elaborated and sent to the board via serial communication with a frequency of 100 Hz. The command acquired by the joystick has been elaborated in order to convert a desired bending direction into PWM values applied to the actuators, maximum currents of 0.6 A have been employed. The tests have been conducted with an room temperature of 22° C , actuation time have been evaluated around 1 second. Forced ventilation has been employed to speed-up the cooling process.

Obtaining a feedback on platform pose and employing the inverse kinematics, to perform position closed loop control will be part of future works and it is not within the aims of this paper.

Elaborating camera recordings (5Mpxl digital camera, SONY, Japan) with a simple segmentation algorithm, actuation range of SA and PA configurations has been obtained for both bending and squeezing DOFs.

The gripper has been assembled placing the compliant component at the top of the PTFE tube, the actuator running inside the tube has been constrained at the bottom component of the parallel module (Fig 12 center). Gripper actuation range has been verified.

Finally, the whole device has been assembled (Fig.12 right) and the conversion of the parallel module squeezing motion to a gripper roll motion thanks to the twisting module has been evaluated.

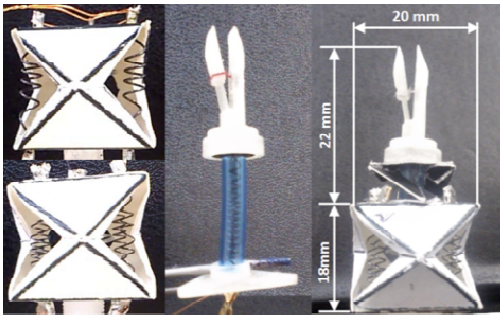

Figure 12. Prototypes produced for components and system performace evaluation. Parallel module SA (left top) and PA (left bottom). Compliant gripper (center). 4 DOFs wrist integrating all the system components including the twisting module.

III. RESULTS AND DISCUSSION

Actuation range of the squeezing DOF for the parallel module in SA and PA configuration has been evaluated as 5.2 mm and 6.1mm respectively,

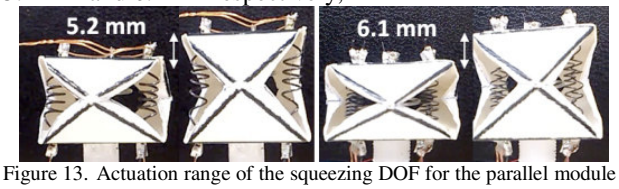

Figure 13. Actuation range of the squeezing DOF for the parallel module in SA (left) and PA (right) configurations .

While angular range in platform bending resulted +27/-15 for SA and +27/-20 degrees for PA.

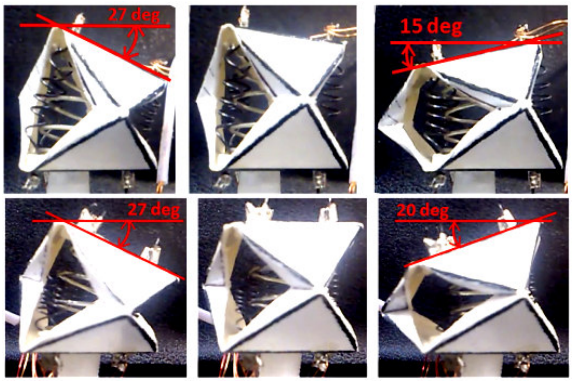

Figure 14. Actuation range of the angle DOF for the parallel module in SA (topline) and PA (bottom line) configurations.

The compliant gripper has been actuated successfully, but due to the low elasticity of the rapid prototyping employed material, the actuation range resulted quite small; furthermore the employed PTFE tube decreases thermal exchanges increasing the cooling time of the alloy.

Finally, the complete prototype has been assembled and the gripper roll angular range has been evaluated. The PA configuration of the parallel module has been employed since provides wider actuation range; for a squeezing motion of 6 mm the corresponding roll motion has been around 70 degrees.

In the final prototype, a reduction of the parallel module actuation range has been noticed due to the quite high stiffness of the PTFE tube.

IV. Conclusion and Future Works

In this paper a SMA actuated, miniaturized, origami-enabled, parallel structure is presented as a versatile module for novel robotic tool in MIS; moreover, the parallel module has been coupled with a novel twisting module and a compliant gripper obtaining a 4-DOFs miniaturized end-effector.

The proposed design approach has the advantage to generate scalable devices avoiding the need of simplifying mechanisms or scarifying robot dexterity. Inherent compliance is one of the most important characteristics of the proposed system both in the structure itself and on the actuation system.

The proof of concept of the proposed system shows promising results, although actuation system has not been optimized and more effective actuation configurations can be designed.

Inverse kinematics considering degrees of freedom couplings i.e. contemporary twisting and bending motion, jointly with optimized design and scalability of the technology will be the focus of future works, SCM fabrication technique will be considered a reference point.

References

[1] Champagne B, Stulberg JJ, Fan Z, Delaney CP. The feasibility of laparoscopic colectomy in urgent and emergent settings. Surg Endosc 2008; 23(8): 1791 – 1796

[2] Asakuma M, Perretta S, Allemann P, et al. (2009) Challenges and lessons learned from NOTES cholecystectomy initial experience: a stepwise approach from the laboratory to clinical application. Journal of Hepatobiliary Surgery 16: 249–254.

[3] A. Lehman, N. Wood, S. Farritor, M. Goede, and D. Oleynikov, Dexterous miniature robot for advanced minimally invasive surgery, Surgical Endoscopy, vol. 25, pp. 119–123, Jan. 2011.

[4] Tognarelli, S., Salerno, M., Tortora, G., Quaglia, C., Dario, P., & Menciassi, A. (2012, June). An endoluminal robotic platform for Minimally Invasive Surgery. In Biomedical Robotics and Biomechatronics (BioRob), 2012 4th IEEE RAS & EMBS International Conference on (pp. 7-12). IEEE.

[5] Dupont, P. E., Lock, J., Itkowitz, B., & Butler, E. (2010). Design and control of concentric-tube robots. Robotics, IEEE Transactions on, 26(2), 209-225.

[6] J. Shang, C. J. Payne, J. Clark, D. P. Noonan, K.-W. Kwok, A. Darzi, and G.-Z. Yang, "Design of a multitasking robotic platform with flexible arms and articulated head for minimally invasive surgery," in Proc. IEEE/RSJ Int. Conf. Intelligent Robots and Systems, 2012, pp. 1988–1993.

[7] Bajo, A., Dharamsi, L., Netterville, J. L., Garrett, G. C. & Simaan, N (2013). Robotic-Assisted Micro-Surgery of Throat: the Trans-Nasal Approach. In Appected for publication in IEEE International Conference on Robotics and Automation (ICRA'2013).

[8] LM Dharamsi, A Bajo, JL Netterville, CG Garrett, N Simaan A Telerobotic System for Transnasal Surgery of the Larynx and Upper Airways Otolaryngology--Head and Neck Surgery 149 (2 suppl), P89-P90

[9] Vitiello, V.; Su-Lin Lee; Cundy, T.P.; Guang-Zhong Yang, "Emerging Robotic Platforms for Minimally Invasive Surgery," Biomedical Engineering, IEEE Reviews in , vol.6, no., pp.111,126, 2013

[10] Shang, J., Noonan, D. P., Payne, C., Clark, J., Sodergren, M. H., Darzi, A., & Yang, G. Z. (2011, May). An articulated universal joint based flexible access robot for minimally invasive surgery. In Robotics and Automation (ICRA), 2011 IEEE International Conference on (pp. 1147-1152). IEEE.

[11] Salerno, M., Tognarelli, S., Quaglia, C., Dario, P., & Menciassi, A. (2013). Anchoring frame for intra-abdominal surgery. The International Journal of Robotics Research, 32(3), 360-370.

[12] Follador, M., M. Cianchetti, and C. Laschi. "Development of the functional unit of a completely soft octopus-like robotic arm." Biomedical Robotics and Biomechatronics (BioRob), 2012 4th IEEE RAS & EMBS International Conference on. IEEE, 2012.

[13] Cho, K. J., Koh, J. S., Kim, S., Chu, W. S., Hong, Y., & Ahn, S. H. (2009). Review of manufacturing processes for soft biomimetic robots. International Journal of Precision Engineering and Manufacturing, 10(3), 171-181.

[14] Wood, R. J., Avadhanula, S., Sahai, R., Steltz, E., & Fearing, R. S. (2008). Microrobot design using fiber reinforced composites. Journal of Mechanical Design, 130, 052304.

[15] K. Zhang and J. S. Dai, (2013). Classification of Origami Evolved Foldable Linkages and Emerging Applications, ASME 2013 International Design Engineering Technical Conferences & Computers and Information in Engineering Conference, Portland, USA.

[16] Fischer, H., Vogel, B., & Welle, A. (2004). Applications of shape memory alloys in medical instruments. Minimally Invasive Therapy & Allied Technologies, 13(4), 248-253.

[17] Ho, M., McMillan, A. B., Simard, J. M., Gullapalli, R., & Desai, J. P. (2012). Toward a meso-scale SMA-actuated MRI-compatible neurosurgical robot. Robotics, IEEE Transactions on, 28(1), 213-222.

[18] K. Zhang, Y. Fang, J. S. Dai and H. Fang, (2010). Geometry and Constraint Analysis of the 3-Spherical Kinematic Chain Based Parallel Mechanism, ASME Transactions, Journal of Mechanism and Robotics, 2(3).

[19] Simaan, N., Taylor, R., & Flint, P. (2004, April). A dexterous system for laryngeal surgery. In Robotics and Automation, 2004. Proceedings. ICRA'04. 2004 IEEE International Conference on (Vol. 1, pp. 351-357). IEEE.

[20] An, S. M., Ryu, J., Cho, M., & Cho, K. J. (2012). Engineering design framework for a shape memory alloy coil spring actuator using a static two-state model. Smart Materials and Structures, 21(5), 055009.

[21] Kim, H., Han, Y., Lee, D. Y., Ha, J. I., & Cho, K. J. (2013). Sensorless displacement estimation of a shape memory alloy coil spring actuator using inductance. Smart Materials and Structures, 22(2), 025001.

[22] Noh, M., Kim, S. W., An, S., Koh, J. S., & Cho, K. J. (2012). Flea-inspired catapult mechanism for miniature jumping robots. In Proc. Int. Workshop on Bio-Inspired Robots.